Estimation of the Under-Ice Acoustic Field in AUV Communication Networks

Wensheng Sun, Chaofeng Wang, Zhaohui Wang, and Min Song
Michigan Technological University, Houghton, MI 49931, USA
{wsun3,cwang8,zhaohuiw,mins}@mtu.edu

ABSTRACT

Autonomous underwater vehicles (AUVs) are the platform of choice for ocean exploration and surveillance in the ice-covered regions. Due to the large attenuation of radio signals in water, acoustic communications have been the major technique for underwater wireless information transfer. In the under-ice environment, the acoustic propagation is largely determined by a stratified sound speed profile (SSP) and the ice-reflection characteristics. Based on the ray theory, this work develops an inversion algorithm to estimate the SSP and the ice reflection coefficient via an iterative method. The acoustic measurements collected during data transmission within the AUV network, including the propagation delay and the amplitude of the received signal along each eigen path, are used for the inversion. With the estimated SSP and the ice-reflection coefficient, the under-ice acoustic field can then be constructed to guide future acoustic communications among the AUVs. The proposed algorithm is evaluated via Bellhop synthesized data and achieves decent accuracy in the SSP and the ice-reflection coefficient estimation.

KEYWORDS

Autonomous underwater vehicle, sound speed profile, ray theory, under-ice, reflection coefficient.

ACM Reference Format:
Wensheng Sun, Chaofeng Wang, Zhaohui Wang, and Min Song. 2017. Estimation of the Under-Ice Acoustic Field in AUV Communication Networks. In *WUWNET'17: WUWNET'17: International Conference on Underwater Networks & Systems, November 6–8, 2017, Halifax, NS, Canada.* ACM, New York, NY, USA, 5 pages. https://doi.org/10.1145/3148675.3148711

1 INTRODUCTION

Autonomous underwater vehicles (AUVs) have been extensively used for ocean and inland lake exploration, oil and gas drilling, and environment monitoring [8], particularly in the ice-covered regions. Due to the large attenuation of radio signals in water, acoustic waveforms are typically used for underwater wireless information transfer and AUV navigation control.

Relative to the open-water acoustic environment, the under-ice acoustic environment exhibits unique characteristics. First, the under-ice environment features an upper-refracting sound speed profile (SSP) which along with the ice cover, yields surface-ducted sound propagation [10]. Secondly, with the ice cover as a rigid reflector, the under-ice acoustic channel is much more stable than its open-water counterpart with large surface dynamics. Thirdly, the under-ice ambient noise level is lower than that in open water, and is characterized by spiky ice cracking noise. The stationarity of the under-ice acoustic channel and the low ambient noise level allow efficient inversion of the water environment parameters, such as the SSP and the ice-reflection coefficient.

The knowledge of the SSP is critical for AUVs to make informative navigational decisions and choose appropriate acoustic communication strategies. However, the SSP varies with the water environment parameters such as the salinity and the temperature. It is often inefficient for an AUV to measure the SSP online, as it is required to navigate through the whole water column.

Inversion of the SSP has been studied based on acoustic measurements from vertical or horizontal hydrophone arrays. In [5], a linearization technique is developed based on the ray theory to estimate the SSP and the source location. In [3], a state-space model is proposed based on the normal mode theory to estimate the SSP recursively. The compressive sensing technique is recently applied for the SSP estimation in [1]. A matched field processing method is developed in [6] to estimate the reflection amplitudes and phases by the Arctic ice.

Different from most existing works that focus on the SSP inversion in *range-independent* environments using acoustic measurements collected by hydrophone arrays, this work takes the acoustic measurements obtained during acoustic communications among an AUV network for the inversion. The spatial distribution of the AUVs in the water area of interest allows the estimation of the three-dimensional sound speed field which may be *range-dependent.* In this work, we develop an inversion algorithm to estimate the range-dependent SSP and the surface reflection coefficient in the under-ice environment. A basis-expansion model is introduced to parameterize the range-dependent sound speed field. The acoustic measurements at receiving AUVs, specifically, the propagation delay and the amplitude of the received signal along each eigen path, are used for the inversion. Based on the ray theory [9], the problem is formulated as a nonlinear optimization problem, and is solved via an interior point method [2]. For a given source node, the estimated SSP and the ice-reflection coefficient allow the construction of the sound pressure field, which enables informative decision-making on AUV navigation and acoustic communication strategies. The performance of the proposed algorithm is validated via Monte Carlo simulations.

WUWNET'17, November 6–8, 2017, Halifax, NS, Canada

ACM ISBN 978-1-4503-5561-2/17/11…$15.00
https://doi.org/10.1145/3148675.3148711

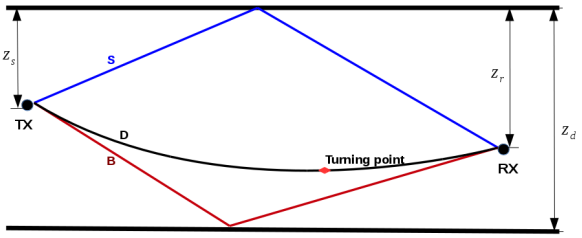

Figure 1: Illustration of the acoustic paths

2 PROBLEM FORMULATION

An underwater acoustic channel can be represented as

$$h(\tau) = \sum_{n=1}^{N_{\text{pa}}} a_n \delta(\tau - \tau_n), \tag{1}$$

where N_{pa} is the number of paths, a_n and τ_n represent the amplitude and the delay of the nth path, respectively. In open-water acoustic channels, a_n and τ_n could be time-varying. However, as justified in the introduction, it is reasonable to assume a time-invariant channel in the under-ice environment.

Due to the reflection and refraction of different propagation traces, different paths, such as direct path (D), the first surface-bounced path (S) and the first bottom-bounced path (B), will experience different signal losses and propagation delays. According to the ray theory, each ray is characterized by the ray parameter p defined as

$$p = \frac{\cos(\theta_{\text{s}})}{c(z_{\text{s}}, 0)} = \frac{\cos(\theta)}{c(z, r)}, \tag{2}$$

where θ is the grazing angle of the ray at a certain location, $c(z, r)$ is the range dependent sound speed at depth z and horizontal distance r, the subscript s represents the corresponding variables at the source location. Dividing an area into J regions, the range-dependent SSP can be approximated by the weighted summation of empirical orthogonal functions (EOFs) as

$$c(z, r) = \bar{c}(z, r) + \sum_{i=1}^{N_{\text{b}}} \sum_{j=1}^{J} \gamma_{i,j} \phi_i(z) \psi_j(r), \tag{3}$$

where N_{b} is the number of basis functions for the approximation, $\gamma_{i,j}$ is the weight of ith EOF ϕ_i in the jth region, where the basis functions can be obtained from the sound speed covariance matrix [5]. $\psi_j(r)$ is a rectangular function, which equals to 1 in the jth region and 0 elsewhere. $\bar{c}(z, r)$ is the mean SSP and is obtained from the empirical measurements. Define $\boldsymbol{\gamma} = [\gamma_{1,1}, \gamma_{1,2}, \cdots, \gamma_{N_{\text{b}},J}]^{\text{T}}$, the range-dependent SSP can be represented as a function of the EOF coefficient vector, $c(\boldsymbol{\gamma})$.

The amplitude a and the propagation delay τ of each path in (1) are determined by the locations of the transmitter and the receiver and the SSP $c(\boldsymbol{\gamma})$. Affected by either the reflections or the refraction, a ray can be divided into several segments by the turning points where the ray changes its vertical direction. As demonstrated in Fig. 1, the paths S and B have turning points at the surface and bottom respectively due to the reflection. The direct path D depicts the possibility of a turning point purely caused by the refraction. More often than not, the refraction-caused turning point does not exists in path D. The following calculations related to path D are based on this assumption. Otherwise, subsection integral should be carried out accordingly.

Define z_{j-1} and z_j as the depths of the starting point and the ending point of the ray in the jth region, where $j = [1, 2, \cdots, J]$, and $z_0 = z_{\text{s}}$ and $z_J = z_{\text{r}}$ are the depths of the source and the receiving node, respectively. In addition, z_{j-1} and z_j are related by the horizontal distance r_j of the jth ray segment as

$$r_j = \int_{z_{j-1}}^{z_j} \frac{p c_j(z)}{\sqrt{1 - p^2 c_j(z)^2}} dz. \tag{4}$$

Assuming the reflections of path B and path S happened in the mth and nth region, respectively, the τ's can be found by [7]

$$\tau_{\text{D}} = \sum_{j=1}^{J} \int_{z_{j-1}}^{z_j} \frac{1}{c_j(z)\sqrt{1 - p_{\text{D}}^2 c_j^2(z)}} dz, \tag{5}$$

$$\begin{aligned}\tau_{\text{B}} = &\sum_{j=1, j\neq m}^{J} \int_{z_{j-1}}^{z_j} \frac{1}{c_j(z)\sqrt{1 - p_{\text{B}}^2 c_j^2(z)}} dz \\ &+ \int_{z_{m-1}}^{z_{\text{d}}} \frac{1}{c_m(z)\sqrt{1 - p_{\text{B}}^2 c_m^2(z)}} dz + \int_{z_m}^{z_{\text{d}}} \frac{1}{c_m(z)\sqrt{1 - p_{\text{B}}^2 c_m^2(z)}} dz,\end{aligned} \tag{6}$$

$$\begin{aligned}\tau_{\text{S}} = &\sum_{j=1, j\neq n}^{J} \int_{z_{j-1}}^{z_j} \frac{1}{c_j(z)\sqrt{1 - p_{\text{S}}^2 c_j^2(z)}} dz \\ &+ \int_{0}^{z_{n-1}} \frac{1}{c_n(z)\sqrt{1 - p_{\text{S}}^2 c_n^2(z)}} dz + \int_{0}^{z_n} \frac{1}{c_n(z)\sqrt{1 - p_{\text{S}}^2 c_n^2(z)}} dz,\end{aligned} \tag{7}$$

where the equivalent SSP in the jth region is expressed as $c_j(z) = \bar{c}(z) + \sum_{i=1}^{N_{\text{b}}} \gamma_{i,j} \phi_i(z)$. z_{d} represents the depth of the water column.

Similarly, the path length along each ray can be found as

$$d_{\text{D}} = \sum_{j=1}^{J} \int_{z_{j-1}}^{z_j} \frac{1}{\sqrt{1 - p_D^2 c_j^2(z)}} dz, \tag{8}$$

$$\begin{aligned}d_{\text{B}} = &\sum_{j=1, j\neq m}^{J} \int_{z_{j-1}}^{z_j} \frac{1}{\sqrt{1 - p_{\text{B}}^2 c_j^2(z)}} dz \\ &+ \int_{z_{m-1}}^{z_{\text{d}}} \frac{1}{\sqrt{1 - p_{\text{B}}^2 c_m^2(z)}} dz + \int_{z_m}^{z_{\text{d}}} \frac{1}{\sqrt{1 - p_{\text{B}}^2 c_m^2(z)}} dz,\end{aligned} \tag{9}$$

$$\begin{aligned}d_{\text{S}} = &\sum_{j=1, j\neq n}^{J} \int_{z_{j-1}}^{z_j} \frac{1}{\sqrt{1 - p_{\text{S}}^2 c_j^2(z)}} dz \\ &+ \int_{0}^{z_{n-1}} \frac{1}{\sqrt{1 - p_{\text{S}}^2 c_n^2(z)}} dz + \int_{0}^{z_n} \frac{1}{\sqrt{1 - p_{\text{S}}^2 c_n^2(z)}} dz,\end{aligned} \tag{10}$$

Considering a point acoustic source, the amplitude of each ray can be expressed as

$$a_{\mathrm{D}} = a_{\mathrm{s}}\sqrt{d_{\mathrm{D}}^{-\beta}e^{-\alpha d_{\mathrm{D}}}}, \tag{11}$$

$$a_{\mathrm{B}} = a_{\mathrm{s}}R_{\mathrm{B}}(\theta)\sqrt{d_{\mathrm{B}}^{-\beta}e^{-\alpha d_{\mathrm{B}}}}, \tag{12}$$

$$a_{\mathrm{S}} = a_{\mathrm{s}}R_{\mathrm{S}}(\theta)\sqrt{d_{\mathrm{S}}^{-\beta}e^{-\alpha d_{\mathrm{S}}}}, \tag{13}$$

where a_{s} is the amplitude at the source, and the term $d^{-\beta}$ captures the spreading loss. β is the spreading factor whose practical value is taken as 1.5. $R(\theta)$ is the reflection coefficient of either the top or the bottom interface and it depends on the grazing angle θ at top or bottom boundary [6], which can be found using (2). Dependence of R on the grazing angle could be linear, quadratic or square root [6], and the quadratic form is used as $R(\theta) = 1 - g\theta^2$. The term $e^{-\alpha d}$ represents the absorption loss and α is the frequency dependent attenuation coefficient which can be found according to the Thorp formula [4].

For notation convenience, we group parameters of the same category into vectors, i.e., $\mathbf{a} = [a_{\mathrm{D}}, a_{\mathrm{S}}, a_{\mathrm{B}}]^{\mathrm{T}}$, $\boldsymbol{\tau} = [\tau_{\mathrm{D}}, \tau_{\mathrm{S}}, \tau_{\mathrm{B}}]^{\mathrm{T}}$, $\mathbf{g} = [g_{\mathrm{S}}, g_{\mathrm{B}}]^{\mathrm{T}}$ and stack all the ray parameters into $\mathbf{p}$. Assuming prior knowledge of the source and the receiver locations $(z_{\mathrm{s}}, z_{\mathrm{r}}, r)$, and the EOFs $\boldsymbol{\phi}$ of the SSP, we can represent the amplitudes and the delays as generic functions of the EOF coefficients $\boldsymbol{\gamma}$ and the reflection coefficient constants $\mathbf{g}$, respectively,

$$\begin{aligned} \mathbf{a} &= \mathbf{f}(\mathbf{g}, \boldsymbol{\gamma}), \\ \boldsymbol{\tau} &= \mathbf{h}(\boldsymbol{\gamma}). \end{aligned} \tag{14}$$

Our goal is to estimate the reflection coefficients $\mathbf{R}$ and the SSP expansion coefficients $\boldsymbol{\gamma}$ using the delay and amplitude measurements. Thus, the underwater acoustic pressure field estimation can be obtained.

With an synchronized AUV network of m nodes distributed in an area, the amplitude information $\mathbf{a}$, the delay information $\boldsymbol{\tau}$ can be easily extracted from the acoustic waveform recorded by the nodes. The number of independent amplitude and delay measurements is $m(m-1)/2$, assuming the reciprocity of the channel [11]. The problem is well-defined as long as the number of measurements is greater than the number of unknowns, which is usually the case. Stacking all the measurements into $\mathbf{y}$ and the unknown parameters into $\mathbf{x}$, the unknown parameters can be found by minimizing the least square error,

$$\begin{aligned} &\mathbf{x}_{\mathrm{opt}} = \arg\min_{\mathbf{x}} ||\Theta(\mathbf{x}) - \mathbf{y}||^2, \\ &\text{subject to} \quad 1 - p_k c(\boldsymbol{\gamma}) > 0, \end{aligned} \tag{15}$$

where $\Theta(\mathbf{x})$ represents the functions capturing the relationship between the measurements and the unknowns as shown in (14), p_k is the ray parameter corresponding to the kth measurement, which refers to a path between a node pair. The constraints are applied to guarantee that the integrands in (5) and (8) are real.

3 THE ALGORITHM FOR SSP AND REFLECTION COEFFICIENT ESTIMATION

The optimization problem (15) is a nonlinear optimization problem including integration over the water depth. The estimation of the SSP requires the knowledge of the ray parameters $\mathbf{p}$, vice versa. Thus we propose an algorithm to iteratively estimate the ray parameters and the SSP, where we take turn to treat one as known and estimate the other. Specifically, given the prior SSP estimation $c(\hat{\boldsymbol{\gamma}}^{(i-1)})$ and the corresponding horizontal range r in the ith iteration, the ray parameters are estimated via finding p such that the calculated horizontal distance $r(p, c(\hat{\boldsymbol{\gamma}}^{(i-1)}))$ approaches the known horizontal distance r [7]. The $r(p, c(\hat{\boldsymbol{\gamma}}^{(i-1)}))$ for different paths can be found similarly as (5)-(7), except that the integrand becomes the one used in (4).

In another word, the ray parameters in $\mathbf{p}$ can be estimated via solving the optimization problem,

$$\begin{aligned} &\hat{\mathbf{p}}^{(i)} = \arg\min_{\mathbf{p}} ||\mathbf{r} - \mathbf{r}(\mathbf{p}, c(\hat{\boldsymbol{\gamma}}^{(i-1)}))||^2, \\ &\text{subject to} \quad 0 < p < \frac{1}{c(\hat{\boldsymbol{\gamma}}^{(i-1)})_{min}}, \end{aligned} \tag{16}$$

The constraint is set according to the definition of the ray parameter in (2), $c(\hat{\boldsymbol{\gamma}}^{(i-1)})_{\min}$ is the minimum speed of the previously estimated SSP.

Given the estimated ray parameters, the estimation of the SSP can be cast as an optimization problem,

$$\begin{aligned} &\hat{\boldsymbol{\gamma}}^{(i)} = \arg\min_{\boldsymbol{\gamma}} ||\mathbf{y} - \Theta(\hat{\mathbf{p}}^{(i)}, c(\boldsymbol{\gamma}))||^2, \\ &\text{subject to} \quad 1 - \hat{p}_k^{(i)} c(\boldsymbol{\gamma}) > 0. \end{aligned} \tag{17}$$

The iteration stops when the tolerance threshold is met.

Both the optimization problems of (16) and (17) can be solved by the primal-dual interior point method [2]. In general, the algorithm first introduces a logarithmic barrier function to associate the original objective function and the nonlinear constraints via the Lagrange multiplier method. The original problem is approximated by jointly finding the primal and the dual variables which minimize the barrier function. The update of the variables can be obtained by the Newton's method. For detailed theory, please refer to [2].

4 THEORETIC BASICS FOR ACOUSTIC PRESSURE FIELD RECONSTRUCTION

After obtaining the estimated SSP and the reflection coefficients, the acoustic pressure field $P(\mathbf{u})$ at a certain frequency in a Cartesian coordinate system can be reconstructed according to the ray theory [4]. Starting from the Helmholtz equation,

$$\nabla^2 P + \frac{\omega^2}{c(\mathbf{u})^2} P = -\delta(\mathbf{u} - \mathbf{u}_0), \tag{18}$$

where ω is the acoustic frequency in radiance and $\mathbf{u}_0$ is the source location. With proper boundary conditions, the acoustic pressure field can be derived and expressed as a summation of the ray series,

$$P(\mathbf{u}) = e^{j\omega} \sum_{i=0}^{\infty} \frac{A_i(\mathbf{u})}{(j\omega)^i}, \tag{19}$$

where $A_i(\mathbf{u})$ is the amplitude of the ith ray at location $\mathbf{u}$. In practice, the constructed acoustic pressure field is summed over finite number of rays. More detailed information can be found in [4]. Moreover, the transmission loss can be obtained from the reconstructed

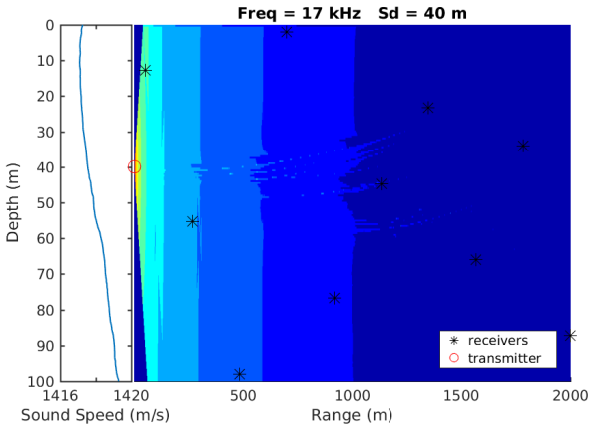

Figure 2: Simulation setup

acoustic pressure field as

$$\mathrm{TL}(\mathbf{u}) = -20 \log \frac{|P(\mathbf{u})|}{|P(\mathbf{u}_r)|}, \tag{20}$$

where $\mathbf{u}_r$ is the reference pressure level measurement location and is usually 1 m away from the source.

5 SIMULATION

5.1 Simulation setup

The proposed algorithm is evaluated by 200 Monte Carlo simulations using Bellhop [9]. In each run, an AUV network of 10 nodes are randomly distributed within an shallow water area, where the maximum distance is 2000 m and the water column depth is 100 m. Without loss of generality, only the channel measurements associated with a common source node is considered. The location of the source node is fixed at 40 m throughout the simulation. In practice, each sensor node can act as both a transmitter and a receiver, thus more measurements can be collected. The emitting angle of the source is $[-45, 45]$ degree. The working frequency of the nodes is 17 kHz. The SSP is generated according to (3) using fixed EOFs, and the coefficients of the EOFs are randomly generated within fixed upper and lower bounds following the uniform distribution. The cubic spline is applied to smoothing the SSPs. The top and bottom reflection coefficients are assumed quadratic and the reflection coefficients at 10 degree for the top and bottom boundary are 0.99 and 0.92, respectively. Fig. 2 shows one realization of the geometry of the AUV network along with the SSP and the acoustic field generated by the transmitter. The circle represents the fixed source node and the stars are the randomly distributed receiving nodes in the network.

The normalized mean square error (NMSE) defined as

$$\mathrm{NMSE} = \frac{\|(\mathbf{y} - \hat{\mathbf{y}})\|_2^2}{\|\mathbf{y}\|_2^2}$$

is used as the error metric for the estimated parameters, where $\|.\|_2$ is the l-2 norm.

5.2 Parameter estimation results

Fig. 3 illustrates the accuracy of the estimated unknown system parameters including the normalized absolute error of the ice and the bottom reflection coefficient constants g_S and g_B, the NMSE of the ray parameters $\mathbf{p}$, and the NMSE of the EOF coefficients of the SSP $\boldsymbol{\gamma}$. One can observe that the average errors of g_S and g_B are around 0.2. The main reason of the estimation error for g_S and g_B is that the amplitude measurements are more sensitive to the SSP change than the reflection coefficients according to (12) and (13). The average NMSE of the ray parameter $\mathbf{p}$ is less than 0.001, indicating the considerable accuracy of the estimated $\mathbf{p}$. The NMSEs of the EOF coefficients are less than 0.2 and skewed towards 0.

5.3 SSP estimation results

Fig. 4 shows the histogram of the NMSEs of the estimated SSP. The estimated SSPs are close to the true ones since all the normalized NMSEs are less than 4×10^{-7}. Fig. 5 compares the true SSP with the estimated SSP using the proposed method in one realization. Fig. 4 and Fig. 5 show that the proposed method is able to capture the main trend of true SSP with fluctuations at depths. The fluctuations are closely related to the depths of the nodes in the AUV network. It is expected that sampling more depths will reduce the fluctuations because the integrals in (5) and (8) depend only on the depths of the transmitter and receiver.

5.4 Acoustic pressure field reconstruction and transmission loss

The sound pressure field is reconstructed using the estimated SSP and the boundary reflection coefficients. Quantitative evaluations of the reconstructed acoustic pressure field is performed by calculating the NMSE of the transmission loss at different ranges and depths over all the simulation runs. The data points in Fig. 6(a) is

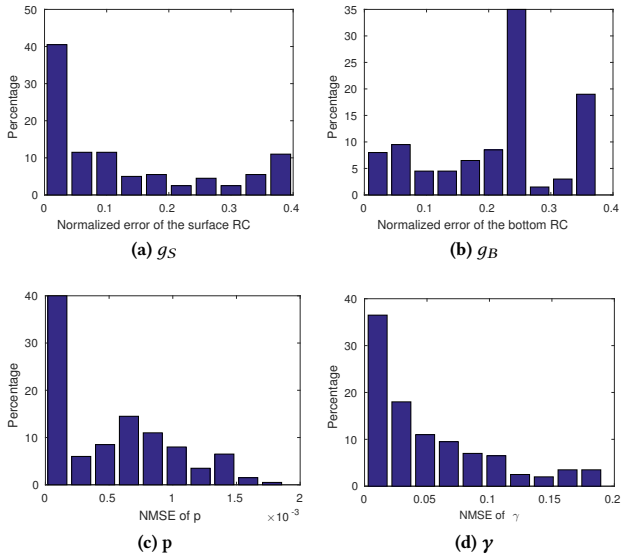

Figure 3: The errors of the estimated parameters

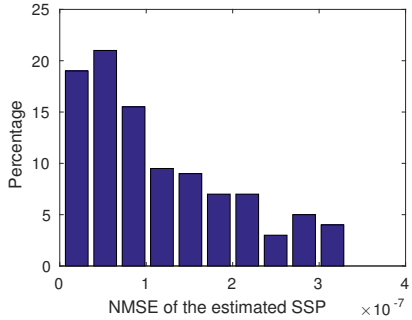

Figure 4: The NMSE of the estimated SSPs

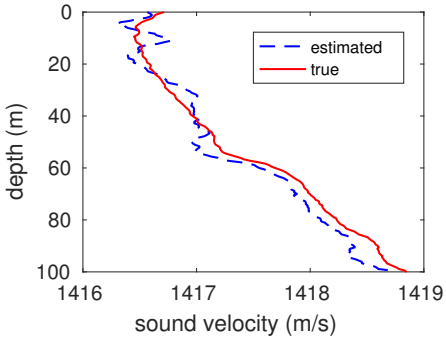

Figure 5: Comparison of the estimated with the true SSP

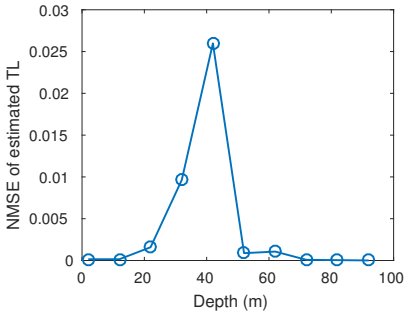

(a) TL versus depth

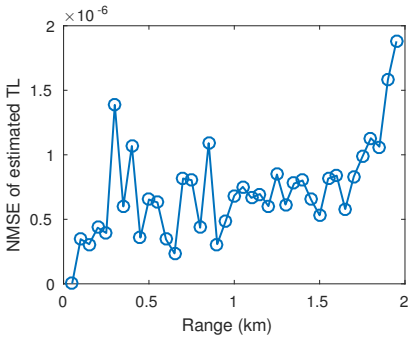

(b) TL versus range

Figure 6: The NMSE of the estimated TL

the average value of the NMSE of the transmission loss at fixed depths. One can observe that the largest error occurs around the source depth 40 m. Because the transmission loss around the source depth is mainly affected by the fragment of the SSP in the same depth region according to (11). Thus the transmission loss is more sensitive to the SSP error. However, the NMSE is less than 0.03, showing the accuracy of the estimated transmission loss. Moreover, Fig. 6b depicts the NMSE of the transmission loss at fixed ranges. It is observed that the reconstruction error slowly increases with range. The maximum NMSE is less than 2×10^{-6}, which shows the accuracy of the estimated transmission loss.

6 CONCLUSIONS

In this work, we developed a ray theory-based iterative method for inversion of the SSP and the ice-reflection coefficient in the under-ice environment, where the acoustic measurements collected during regular acoustic communications among an AUV network are used for the inversion. With the spatial distribution of the AUVs, inversion of the three-dimensional range-dependent sound speed field is achieved through introducing a low-dimensional basis-expansion-based representation. The effectiveness of the proposed algorithm was demonstrated via Monte Carlo simulations. The estimated SSP and the ice-reflection coefficient can be used to compute the sound pressure field and allow informative decision-making on AUV navigation and acoustic communications.

ACKNOWLEDGMENTS

This work was partially supported by the National Science Foundation under Grant Nos.: CNS-1551067 and ECCS-1651135.

REFERENCES

[1] Michael Bianco and Peter Gerstoft. 2016. Compressive acoustic sound speed profile estimation. *The Journal of the Acoustical Society of America* 139, 3 (2016), EL90–EL94.
[2] Stephen Boyd and Lieven Vandenberghe. 2004. *Convex optimization*. Cambridge university press.
[3] James V Candy and E.J Sullivan. 1993. Sound velocity profile estimation: A system theoretic approach. *IEEE journal of oceanic engineering* 18, 3 (1993), 240–252.
[4] Finn B Jensen, William A Kuperman, Michael B Porter, and Henrik Schmidt. 2000. *Computational ocean acoustics*. Springer Science & Business Media.
[5] Tao Lin and Zoi-Heleni Michalopoulou. 2014. Sound speed estimation and source localization with linearization and particle filtering. *The Journal of the Acoustical Society of America* 135, 3 (2014), 1115–1126.
[6] Ellen Livingston and Orest Diachok. 1989. Estimation of average under-ice reflection amplitudes and phases using matched-field processing. *The Journal of the Acoustical Society of America* 86, 5 (1989), 1909–1919.
[7] Xiaoqun Ma. 2001. Efficient inversion methods in underwater acoustics. (2001).
[8] J.W. Nicholson and A.J. Healey. 2008. The present state of autonomous underwater vehicle (AUV) applications and technologies. *Marine Technology Society Journal* 42, 1 (2008), 44–51.
[9] Michael B Porter and Homer P Bucker. 1987. Gaussian beam tracing for computing ocean acoustic fields. *The Journal of the Acoustical Society of America* 82, 4 (1987), 1349–1359.
[10] Wensheng Sun, Chaofeng Wang, Zhaohui Wang, and Min Song. 2015. Experimental Comparison Between Under-Ice and Open-Water Acoustic Channels. In *Proceedings of the 10th International Conference on Underwater Networks & Systems*. ACM, 39.
[11] Wensheng Sun, Zhaohui Wang, M. Jamalabdollahi, and S.A. Reza Zekavat. 2014. Experimental study on the difference between acoustic communication channels in freshwater rivers/lakes and in oceans. In *Proceedings of Asilomar Conf. on Signals, Systems and Computers* (2-5). https://doi.org/10.1109/ACSSC.2014.7094457